

LA-UR-07-0587

*Approved for public release;
distribution is unlimited.*

Title: Approximate local center of mass calculations: application to multi-material interface reconstruction

Author(s): S. P. Schofield, R. Loubere, R. V. Garimella, M. M. Francois

Intended for:



Los Alamos National Laboratory, an affirmative action/equal opportunity employer, is operated by the Los Alamos National Security, LLC for the National Nuclear Security Administration of the U.S. Department of Energy under contract DE-AC52-06NA25396. By acceptance of this article, the publisher recognizes that the U.S. Government retains a nonexclusive, royalty-free license to publish or reproduce the published form of this contribution, or to allow others to do so, for U.S. Government purposes. Los Alamos National Laboratory requests that the publisher identify this article as work performed under the auspices of the U.S. Department of Energy. Los Alamos National Laboratory strongly supports academic freedom and a researcher's right to publish; as an institution, however, the Laboratory does not endorse the viewpoint of a publication or guarantee its technical correctness.

Approximate local center of mass calculations: application to multi-material interface reconstruction

S. P. Schofield¹, R. Loubere², R. V. Garimella¹, M. M. Francois³, and

1. Mathematical Modeling and Analysis (T-7), Los Alamos National Laboratory
2. CNRS and Toulouse University, France
3. Continuum Dynamics (CCS-2), Los Alamos National Laboratory

Abstract

In this article, we explore the calculation of a local (cell based) center of mass derived from a piecewise constant density field. The method utilizes planar and higher order reconstructions of the density field to derive a piecewise continuous functional representation of the density which is then integrated to calculate a local center of mass. We demonstrate this method in the context of multi-material interface reconstruction where the materials are correctly located within a mesh cell with the center of mass calculation based on their respective volume fraction functions. For two-materials, the method is identical to Youngs' method. Second order extensions of the reconstruction method are also presented.

1 Introduction

In finite volume flow simulations, the density of a material is often represented as constant over each mesh cell, where the constant value is equal to the mean value of the density over the cell [9]. High resolution methods rely on deriving a higher order polynomial representation of the density based on the cell average data. In some situations (ELABORATE), it becomes advantageous if the volume of a material within the cell can instead be transformed to a point mass. The obvious point to choose is the center of mass of the material, $\mathbf{x}_m(\mathcal{C}_i)$ within the cell, \mathcal{C}_i , defined as

$$\mathbf{x}_m(\mathcal{C}_i) = \frac{\int_{\mathcal{C}_i} \mathbf{x} \rho(\mathbf{x}) dA}{\int_{\mathcal{C}_i} \rho(\mathbf{x}) dA} \quad (1)$$

However, in many flow simulations, the density is only known as a cell average, that is

$$\bar{\rho}_i = \frac{\int_{\mathcal{C}_i} \rho(\mathbf{x}) dA}{\int_{\mathcal{C}_i} dA} \quad (2)$$

To obtain a functional representation of the density, a reconstruction of the field is performed.

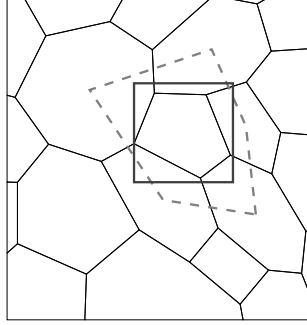


Figure 1: The integration paths used in the calculation. The dashed line is the contour used for the Green-Gauss gradient estimation. The solid line is the bounding square integrated over to find the approximate material centroids from the linear reconstruction of the volume fraction function.

We assume the density is continuous and may be approximated locally by a plane taking the form

$$\tilde{\rho}(\mathbf{x}) = \bar{\rho}_i + \delta \cdot (\mathbf{x} - \mathbf{x}_c(\mathcal{C}_i)) \quad (3)$$

where δ is taken as the gradient of the density and $\mathbf{x}_c(\mathcal{C}_i)$ is the centroid of the mesh cell \mathcal{C}_i defined as

$$\mathbf{x}_c(\mathcal{C}_i) = \int_{\mathcal{C}_i} \mathbf{x} dA \quad (4)$$

The advantage of the representation in Equation 12 is that it preserves the correct mean value, that is

$$\frac{1}{\|\mathcal{C}_i\|} \int_{\mathcal{C}_i} \tilde{\rho}(\mathbf{x}) dA = \bar{\rho}_i \quad (5)$$

The gradient, δ , may be calculated using several methods. A Green-Gauss method [1], where the gradient is estimated by an approximate boundary integral taken over the centroids of all of mesh cells connected by vertex to the cell being reconstructed, is exact for linear functions. The contour path is shown in the dashed line in Figure 1. A least-squares method is also available [10]. We found the Green-Gauss method to provide more consistent results.

The magnitude of the gradient may be quite large. For determining the interface normal this is not an issue as it may be normalized to unit length. However, as the gradient in planar reconstruction of the volume fraction function, it is ill-suited. The planar reconstruction may exceed the local bounds of the density

$$\rho_{\min} \leq \tilde{\rho}(\mathbf{x}) \leq \rho_{\max} \quad (6)$$

where ρ_{\min} and ρ_{\max} are the largest and smallest values of the mean density $\bar{\rho}_j$ in the neighboring cells. To correct this, the Barth-Jepersen limiter [2, 3] is calculated. It gives a scalar $0 < \phi \leq 1$, such that the linear reconstruction with gradient $\phi\delta$ satisfies the local bounds.

Once the limited gradient, $\phi\delta$, has been calculated, the approximate center of mass, is determined by integrating the linear reconstruction:

$$\tilde{\mathbf{x}}_m(\mathcal{C}_i) = \frac{1}{\int_{\mathcal{C}_i} \tilde{\rho}(\mathbf{x}) dA} \int_{\mathcal{C}_i} \mathbf{x} \tilde{\rho}(\mathbf{x}) dA \quad (7)$$

$$= \frac{1}{\|\mathcal{C}_i\| \bar{\rho}_i} \int_{\mathcal{C}_i} \mathbf{x} \{ \bar{\rho}_i + \phi\delta \cdot (\mathbf{x} - \mathbf{x}_c(\mathcal{C}_i)) \} dA \quad (8)$$

The integrals may be evaluated directly using an application of Green's Theorem. Explicit formulas for the integrals of the planar reconstruction over a polygon are provided by S. F. Bockman [6].

2 Application to multi-material interface reconstruction

The volume of fluid method, originally developed by C. W. Hirt and B. D. Nichols [7], advects the fractional volumes of each fluid in the cell to track materials in an incompressible flow simulation. The volume fraction, $f_m(\mathcal{C}_i)$, of a material, m , in a cell, \mathcal{C}_i of volume $\|\mathcal{C}_i\|$ is defined as

$$f_m(\mathcal{C}_i) = \frac{A_m(\mathcal{C}_i)}{\|\mathcal{C}_i\|} \quad (9)$$

where $A_m(\mathcal{C}_i)$ is the volume of the material in the cell.

Fundamental to the method is the idea of interface reconstruction, [4, 5, 10, 11] where the interfaces between materials are located using the volume fractions.

A common problem impacting these reconstruction methods is their dependence on a specified material ordering, i.e. if more than two materials are present in a cell, the reconstruction may depend on the sequence in which the materials are processed. This is undesirable as it may improperly locate materials within the cell. In a finite volume implementation, this may result in material being incorrectly fluxed into neighboring cells.

If we assume a material occupies a connected subset, Ω_m of a mesh cell, \mathcal{C}_i , then the natural representation for the location of a the material is the center-of-mass or centroid of that material region, Ω_m . However, in VOF methods, that information is not generally available. Instead, it must be inferred from the volume fraction function over a region of the mesh surrounding the cell that is to be reconstructed.

The center of mass of material m contained within mesh cell \mathcal{C}_i , is defined as

$$\mathbf{x}_m(\mathcal{C}_i) = \frac{\int_{\mathcal{C}_i} \mathbf{x} \chi_m(\mathbf{x}) d\mathbf{x}}{\int_{\mathcal{C}_i} \chi_m(\mathbf{x}) d\mathbf{x}}, \quad (10)$$

where $\chi_m(\mathbf{x})$ is the characteristic function for material m ,

$$\chi_m(\mathbf{x}) = \begin{cases} 1 & \mathbf{x} \in \Omega_m \\ 0 & \mathbf{x} \notin \Omega_m. \end{cases} \quad (11)$$

Since the volume fraction and cell area are known, the volume integral does not need to be computed, as

$$\int_{\mathcal{C}_i} \chi_m(\mathbf{x}) d\mathbf{x} = \|\mathcal{C}_i\| \bar{f}_m(\mathcal{C}_i) \quad (12)$$

Unfortunately, $\chi_m(\mathbf{x})$ is not known and an approximation to the distribution of the material within the cell must be found. The volume fraction function is similar to a density of a material. As such the application of the method detailed in the previous section is appropriate.

Based on previous results using power diagram based reconstruction for multi-material cells with the true center of mass a material within the cell [12], we utilize the reconstruction strategy here with the calculated center of mass as generators of the power diagram.

2.1 Power diagram based interface reconstruction

Briefly, a power diagram is a generalization of a Voronoi diagram generated from a set of points, S , each with an associated radius or weight. The Laguerre distance from a point $\mathbf{x} \in \mathbb{R}^n$ to a point mass, $s_i \in S$ with $s_i = (\mathbf{x}_i, w_i)$ is defined as

$$d_L^2(\mathbf{x}, s_i) = d^2(\mathbf{x}, \mathbf{x}_i) - w_i \quad (13)$$

where $d^2(\mathbf{x}, \mathbf{x}_i) = \sum_{i=1}^n (x - x_i)^2$ is the usual Euclidean distance. In a power diagram, w_i is replaced with w_i^2 in Equation 13 and the resulting distance is called the power of the point \mathbf{x} with respect to \mathbf{x}_i . This may be interpreted as the distance from the point \mathbf{x} to a point on the circle centered at \mathbf{x}_i with radius w_i along the line through \mathbf{x} that is tangent to that circle.

Each cell in the power diagram is the set of points

$$cell(s_i) = \{\mathbf{x} \in \mathbb{R}^n | d_L(\mathbf{x}, s_i) < d_L(\mathbf{x}, s_j) \forall s_j \in S, s_j \neq s_i\} \quad (14)$$

The power bisector between two points $s_i = (\mathbf{x}_i, w_i)$ and $s_j = (\mathbf{x}_j, w_j)$ is the line perpendicular to the segment connecting the points \mathbf{x}_i and \mathbf{x}_j and is located by finding a point, \mathbf{x}_0 on that segment such that $d_L^2(\mathbf{x}_0, s_i) = d_L^2(\mathbf{x}_0, s_j)$.

The volume fractions can be matched by adjusting the weights of each point generator and checking the area of each cell once it has been clipped to the bounding polygon in which it is contained. This requires the solution of a set of non-linear equations

$$A_m(\omega_1, \dots, \omega_{N_m}) = A_i f_m, \quad m = 1 \dots N_m \quad (15)$$

where $A_m(\omega_1, \dots, \omega_{N_m})$ is the area of the power diagram cell corresponding to material m after it has been clipped by the bounding mesh cell with area A_i . f_m is the volume fraction for material m . The constraint

$$\sum_{m=1}^{N_m} A_m(\omega_1, \dots, \omega_n) = A_i \quad (16)$$

reduces the number of equations to $N_m - 1$. For three or fewer materials, we have been able to demonstrate that given a set of generators and volume fractions, a power diagram reconstruction that matches those volume fractions exists and is unique. While we believe this is true for an arbitrary number of materials, we have been unable to prove it. To obtain a unique solution, one weight is set to a specified value and the $N_m - 1$ other weights are adjusted. A Newton procedure with a finite difference derived Jacobian is used to solve Equation 15.

2.2 Material location through linear reconstruction

The power diagram based reconstruction does not require the point generators to be within the cell being reconstructed. This implies that the domain of integration for calculation of the approximate material centers of mass does not necessarily have to be the mesh cell which we are reconstructing. Indeed, we observed noticeable mesh artifacts on unstructured grids when using the mesh cell as the domain. Instead, a suitable choice of domain is to take the smallest square, $S(\mathcal{C}_i)$ such that $\mathcal{C}_i \subseteq S(\mathcal{C}_i)$ and the centroids of the square are the same as that of the mesh cell, i.e. $\mathbf{x}_c(\mathcal{C}_i) = \mathbf{x}_c(S(\mathcal{C}_i))$. We then define the integration domain $S(\mathcal{C}_i) = \{\mathbf{x} \in \mathbb{R}^2 | x_0 \leq x \leq x_1 \text{ and } y_0 \leq y \leq y_1\}$ with $x_1 - x_0 = y_1 - y_0$ and

$$\mathbf{x}_c(\mathcal{C}_i) = \mathbf{x}_c(S(\mathcal{C}_i)) = \frac{1}{\int_{S(\mathcal{C}_i)} dx dy} \int_{S(\mathcal{C}_i)} \mathbf{x} dx dy = \left(\begin{array}{c} \frac{x_1+x_0}{2} \\ \frac{y_1+y_0}{2} \end{array} \right) \quad (17)$$

An example of this integration domain is shown with the dark solid line in Figure 1.

Since $S(\mathcal{C}_i)$ and \mathcal{C}_i have the same centroid, it follows that

$$\int_{S(\mathcal{C}_i)} \{\bar{f}_m + \delta \cdot (\mathbf{x} - \mathbf{x}_c(\mathcal{C}_i))\} dx dy = \|S(\mathcal{C}_i)\| \bar{f}_m \quad (18)$$

which gives the the approximate center of mass as

$$\tilde{\mathbf{x}}_m = \frac{1}{\|S(\mathcal{C}_i)\| \bar{f}_m} \int_{S(\mathcal{C}_i)} \mathbf{x} \{\bar{f}_m + \delta \cdot (\mathbf{x} - \mathbf{x}_c(\mathcal{C}_i))\} dx dy \quad (19)$$

$$= \mathbf{x}_c(\mathcal{C}_i) + \frac{1}{\|S(\mathcal{C}_i)\| \bar{f}_m} \int_{S(\mathcal{C}_i)} \mathbf{x} \{\delta \cdot (\mathbf{x} - \mathbf{x}_c(\mathcal{C}_i))\} dx dy \quad (20)$$

Consider the case of two materials, m , and n , in a polygonal cell where the gradient of the volume fraction functions f_m and $f_n = 1 - f_m$ for the two materials have been computed and are equal to δ and $-\delta$ respectively. The power diagram reconstruction of the interface for the two materials will have an interface normal aligned with $\tilde{\mathbf{x}}_m - \tilde{\mathbf{x}}_n$, i.e. the line connecting the approximate material centers of mass.

$$\tilde{\mathbf{x}}_m - \tilde{\mathbf{x}}_n = \frac{1}{\|S(\mathcal{C}_i)\|} \frac{1}{\bar{f}_m} \int_{S(\mathcal{C}_i)} \mathbf{x} \tilde{f}_m(\mathbf{x}) dx dy - \frac{1}{\|S(\mathcal{C}_i)\|} \frac{1}{1 - \bar{f}_m} \int_{S(\mathcal{C}_i)} \mathbf{x} (1 - \tilde{f}_m(\mathbf{x})) dx dy \quad (21)$$

$$= \frac{1}{\|S(\mathcal{C}_i)\|} \left(\frac{1}{\bar{f}_m} + \frac{1}{1 - \bar{f}_m} \right) \int_{y_0}^{y_1} \int_{x_0}^{x_1} \mathbf{x} (\delta \cdot (\mathbf{x} - \mathbf{x}_c)) \, dx \, dy \quad (22)$$

$$= \frac{\Delta^2}{12} \left(\frac{1}{\bar{f}_m(1 - \bar{f}_m)} \right) \begin{pmatrix} \delta_x \\ \delta_y \end{pmatrix} \quad (23)$$

where $\Delta = x_1 - x_0 = y_1 - y_0 = \sqrt{\|S(\mathcal{C}_i)\|}$.

So indeed the direction between the two material locations will be aligned with the volume fraction gradient ensuring the method is identical to a Youngs' type method for two materials, that is

$$\delta \times (\tilde{\mathbf{x}}_m - \tilde{\mathbf{x}}_n) = \mathbf{0} \quad (24)$$

If the gradients are not exactly opposite, but instead $\nabla f_m = -\phi \nabla f_n$ with $\phi \in \mathbb{R}$, then the above result still holds, but with a different constant in front of the integral in Equation 23. Using this domain combined with the limiter on the gradient, the points typically lie within the cell being reconstructed, although it is not guaranteed.

2.3 Extensions to second order

In general, the method will not exactly reproduce a straight line interface indicating it is not second order [8]. The LVIRA method performs a local optimization to correct the interface normals. It works by minimizing an objective function that measures the discrepancy between the prescribed volume fractions of a material, f_m and the volume fractions that would result from an extension of the interface in a cell into the neighboring cells f'_m . The same strategy could be use to extends this method to second order.

For each material, the linear reconstruction takes the

$$f_m(\mathbf{x}) = \bar{f}_m(\mathcal{C}_i) + R(\theta_m)\delta \cdot (\mathbf{x} - \mathbf{x}_c(\mathcal{C}_i)) \quad (25)$$

where

$$R(\theta) = \begin{pmatrix} \cos \theta & \sin \theta \\ -\sin \theta & \cos \theta \end{pmatrix} \quad (26)$$

is the rotation matrix corresponding to a rotation by angle θ . The optimization procedure finds a set of angles, $\theta_1, \theta_2, \dots, \theta_n$, corresponding to the materials in the cell, that minimize the objective function

$$E(\theta_1, \theta_2, \dots, \theta_n) = \sum_{m=1}^n \sum_{\mathcal{C}_j \in \mathcal{N}(\mathcal{C}_i)} (f'_m(\mathcal{C}_j; \theta_1, \theta_2, \dots, \theta_n) - f_m(\mathcal{C}_j))^2 \quad (27)$$

where $f'_m(\mathcal{C}_j; \theta_1, \theta_2, \dots, \theta_n)$ is the volume fraction of material m that would be obtained by extending the interfaces for that material from the cell being reconstructed, \mathcal{C}_i into the neighboring cell \mathcal{C}_j . The limited gradient, δ , is retained. In two materials reconstructions, this method is exactly equivalent to LVIRA.

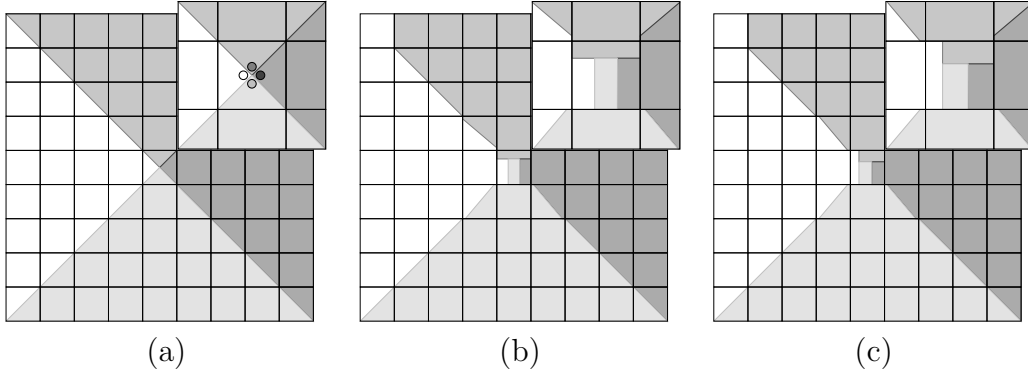


Figure 2: Four material interface reconstruction on an unstructured grid using (a) power diagrams with the reconstructed centroids shown and (b), (c) Youngs' method with two different material orderings.

3 Numerical experiments

Numerical experiments confirm that for two materials examples, the reconstruction is identical to Youngs'. When more than two materials are present, the method correctly locates the position of each material within the cell and provides a reasonable reconstruction. In Figures 2 and 3, the power diagram and reconstructed centroid method is identical to Youngs' in the regions containing only two materials. In the center of each, the method correctly locates each material in the four material cell and provides the appropriate reconstruction. It preserves the symmetry in the structured grid example in Figure 2, but fails to do so on the unstructured grid in Figure 3.

The method does not exactly reproduce a straight line in Figure 3, confirming that, like Youngs' method, it is only first order [8].

In the filament example shown in Figure 4, Youngs reconstruction with the correct material ordering is identical to the power diagram based reconstruction. However, with the incorrect material ordering, white material is placed on the right hand side of the filament, leading to the so called flotsam and jetsam problem with small pieces of material separating off. The power diagram reconstruction does not depend on any material ordering and avoids this problem.

4 Conclusions

We have developed a new, first order material order independent method for interface reconstruction in multi-material cells. It is a natural extension of Youngs method, in that it relies the gradient of the volume fraction function and it is identical to Youngs method in two material cases. For three or more materials, it automatically locates the position of each material in the cell and provides a decomposition of a convex mesh cell into convex regions

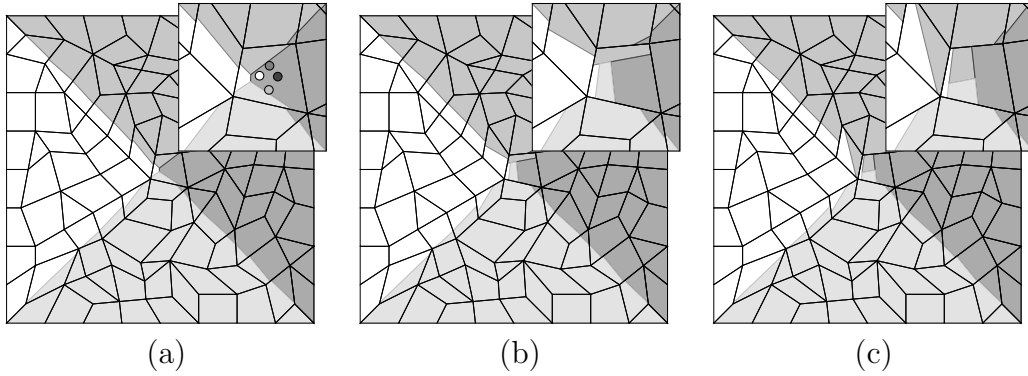


Figure 3: Four material interface reconstruction on an unstructured grid using (a) power diagrams with the reconstructed centroids shown and (b), (c) Youngs' method with two different material orderings.

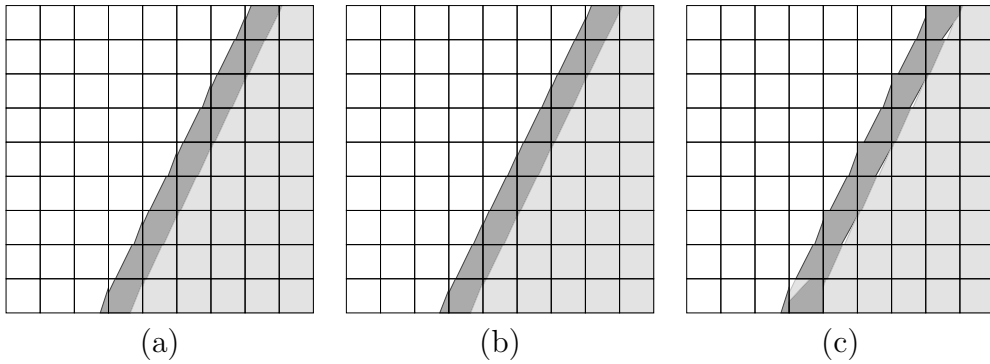


Figure 4: Multi-material interface reconstruction for a filament: (a) reconstructed centroids and power diagrams and (b),(c) Youngs' reconstruction with different material orderings. Notice the presence of the white material on the right hand side of the filament in Youngs' reconstruction in (c). By construction, the power diagram reconstruction is identical to Youngs method in two material cells.

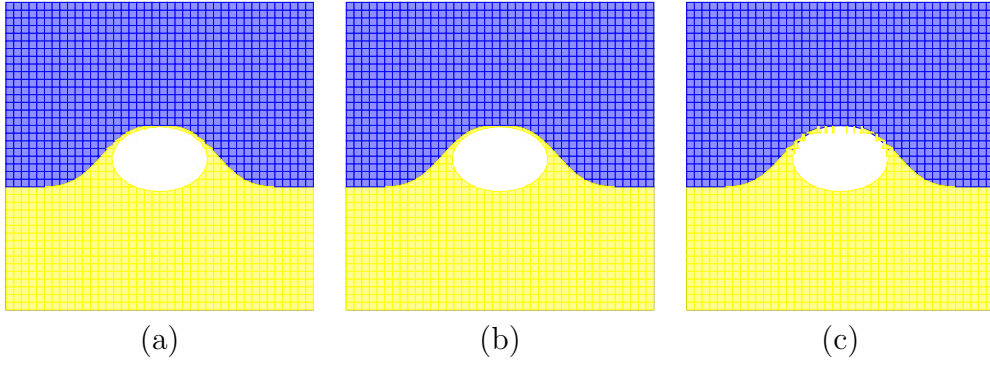


Figure 5: Interface reconstruction for a bubble rising to a free surface. (a) reconstructed centroids and power diagrams and (b),(c) Youngs' reconstruction with different material orderings.

for each material that match the required volume fraction functions.

References

- [1] T. J. Barth, *Aspects of unstructured grids and finite-volume solvers for Euler and Navier-Stokes equations*, VKI/NASA/AGARD Special Course on Unstructured Grid Methods for Advection Dominated Flows AGARD Publication R-787, 1995.
- [2] ———, *Numerical methods for gasdynamics systems*, An introduction to recent developments in theory and numerics for conservation laws, Proceedings of the International School on Theory and Numerics for Conservation Laws (Berlin) (M. Ohlberger D. Kroner and C. Rohde, eds.), Lecture Notes in Computational Science and Engineering, Springer, 1997, pp. 195–285.
- [3] T. J. Barth and D. C. Jespersen, *The design and application of upwind schemes on unstructured meshes*, 27th Aerospace Sciences Meeting, no. AIAA-89-0366, Jan 9-12, 1989.
- [4] D. J. Benson, *Computational methods in Lagrangian and Eulerian hydrocodes*, Computer Methods in Applied Mechanics and Engineering **99** (1992), 235–394.
- [5] ———, *Volume of fluid interface reconstruction methods for multi-material problems*, Applied Mechanics Review **55** (2002), no. 2, 151–165.
- [6] S. F. Bockman, *Generalizing the formula for areas of polygons to moments*, The American Mathematical Monthly **96** (1989), no. 2, 131–132.
- [7] C. W. Hirt and B. D. Nichols, *Volume of fluid (vof) method for the dynamics of free boundaries*, Journal of Computational Physics **39** (1981), 201–225.
- [8] J. E. Pilliod Jr. and E. G. Puckett, *Second-order accurate volume-of-fluid algorithms for tracking material interfaces*, Journal of Computational Physics **199** (2004), 465–502.
- [9] R. L. LeVeque, *Finite volume methods for hyperbolic problems*, Cambridge University Press, Cambridge, UK, 2002.
- [10] W. J. Rider and D. B. Kothe, *Reconstructing volume tracking*, Journal of Computational Physics **141** (1998), 112–152.
- [11] R. Scardovelli and S. Zaleski, *Direct numerical simulation of free-surface and interfacial flow*, Annual Review of Fluid Mechanics **31** (1999), 567–603.
- [12] S. P. Schofield, R. V. Garimella, M. M. Francois, and R. Loubere, *Material order independent interface reconstruction using power diagrams*, International Journal for Numerical Methods in Fluids **submitted**.